Supplementary Information

Automated Electrochemical Oxygen Sensing Using a 3D-Printed Microfluidic Lab-on-a-Chip System

Daniel Kaufman, Steffen Winkler, Christopher Heuer, Ahed Shibli, Alexander Snezhko, Gideon I. Livshits, Janina Bahnemann*, and Hadar Ben-Yoav*

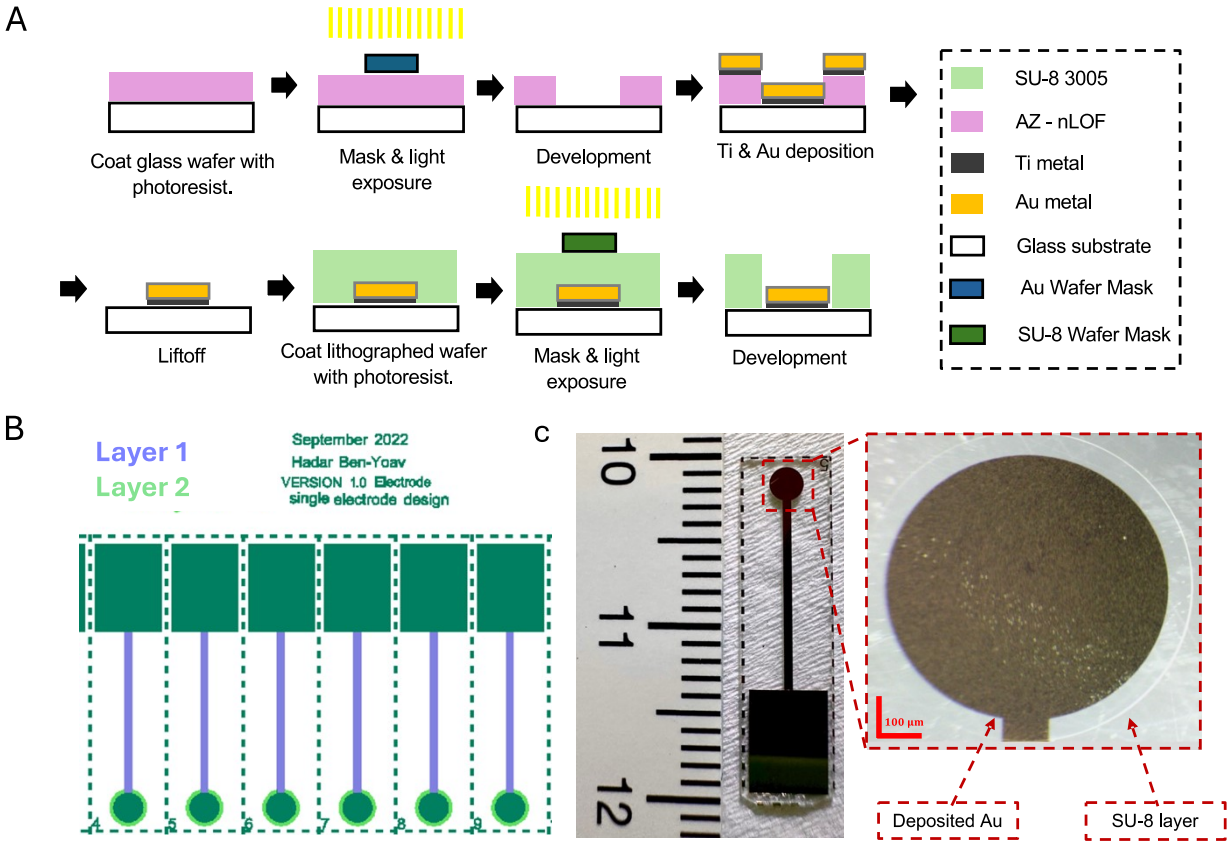

Fig. S1: (A) The microfabrication scheme of a gold electrode: (1) spin-coating the glass wafer with an AZ-nLOF photoresist, (2) exposing the photoresist-coated wafer to a light flux of 8.7 mW/cm² UV light for 18 seconds, followed by a hard-bake (110°C for 1 minute), (3) developing the exposed wafer with AZ-726 MIF for 73 seconds, washing the exposed parts, and creating a pattern, (4) depositing 25 nm of Ti and 250 nm of Au onto the developed wafer, (5) removing the photoresist from the wafer using NMP solution for 30 seconds, leaving the metals deposited in the pattern, (6) spin-coating the lithographed wafer with an SU-8 3005 photoresist, (7) exposing the photoresist-coated wafer to 8.7 mW cm^{-2} UV light for 45.1 seconds, and (8) developing the exposed wafer using PGMA/EBR developer, washing the exposed parts, and creating a pattern, revealing only the active surface area. (B) The design (as seen using Clewin4 software) and (C) a microfabricated gold single electrode with the SU-8-defined chamber, including a 1 mm radius disk electrode connected to 5 mm × 6 mm pads.

To study the PtB/Au morphology and its surface coverage, and in addition to the electrochemical techniques used in this work, the coating geometry was characterized by atomic force microscopy (AFM) and scanning electron microscopy (SEM) tools. SEM imaging revealed that the PtB coating was composed of large continuous areas, each with extended grainy branches that account for a greater effective surface area. The boundaries between the areas are denoted by spaces that appear as black areas in the images. Furthermore, a profilometer along the diameter of the circular electrode reveals the distribution of the heights of these peaks and valleys.

With a rather sharp tip (nominal radius < 8 nm), AFM imaging in non-contact mode revealed the details of the topography. The spaces between the areas can be clearly observed. To calculate the length of the curve, we performed numerical integration along the line profile using WSxM program in Mathematica 14.1 software. The mean ratio was 1.47 ± 0.02, which corresponds to an effective diameter of 1.54 ± 0.02 mm, or an effective surface area of 7.51±0.01 mm^2 (using Eq. S1) – both in complete agreement with the electrochemically calculated surface area using the Randles-Sevcik calculation.

$$(S1)\ A_{effective} = \pi\left(mR * \frac{D_{AuElec}}{2}\right)^2$$

where $A_{effective}$ denotes the calculated effective surface area, mR denotes the mean ratio, and D_{AuElec} denotes the calculated gold electrode diameter. Standard deviation of the linear fit interception; m denotes the slope of the curve.

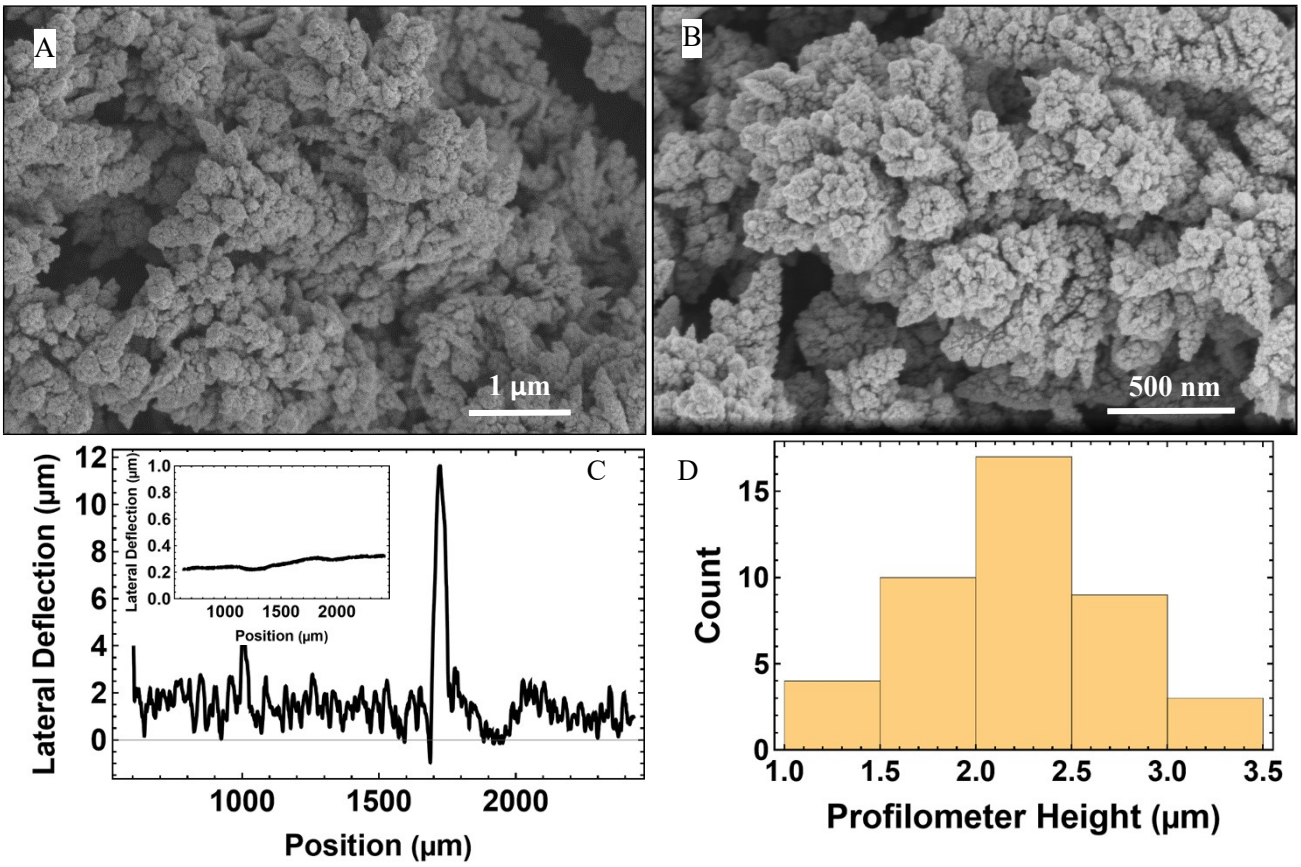

Fig. S2. SEM imaging of the PtB/Au/Glass sample with profilometer data. (A&B) SEM imaging of the PtB coating on the Au electrode. (C) Profilometer data acquired along the diameter of the sample. The peaks and valleys are clearly visible. The inset shows the profile on Au for comparison. (D) Distribution of heights along the profile in (c). The outliers have been removed.

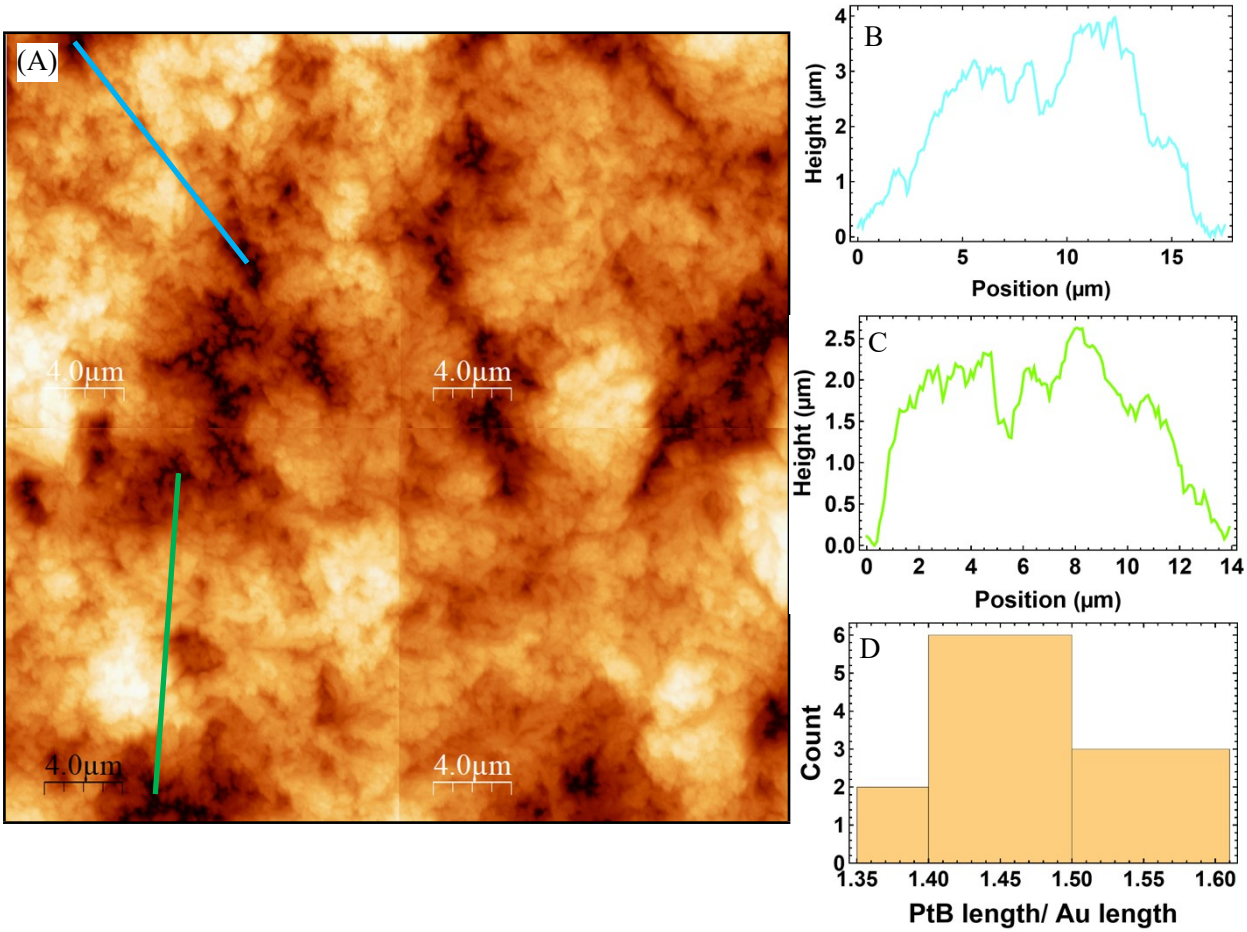

Fig. S3. AFM imaging of the PtB/Au/Glass sample. (A) Four $20\ \mu m\ \times 20\ \mu m$ AFM images (in non-contact mode) collected from adjacent areas and stitched together for a complete view of a $40\ \mu m \times 40\ \mu m$ area. The surface seems to be composed of large mounds or piles of PtB of varying sizes, with boundaries that precipitously drop towards the underlying Au surface. (B&C) Two representative profiles along the blue and green profiles, respectively. For each profile, its length was calculated using path integration along the line profile. (D) Ratio of the length of the PtB profile and the length of the underlying Au base calculated for 11 profiles. Mean ratio = 1.47 ± 0.02.

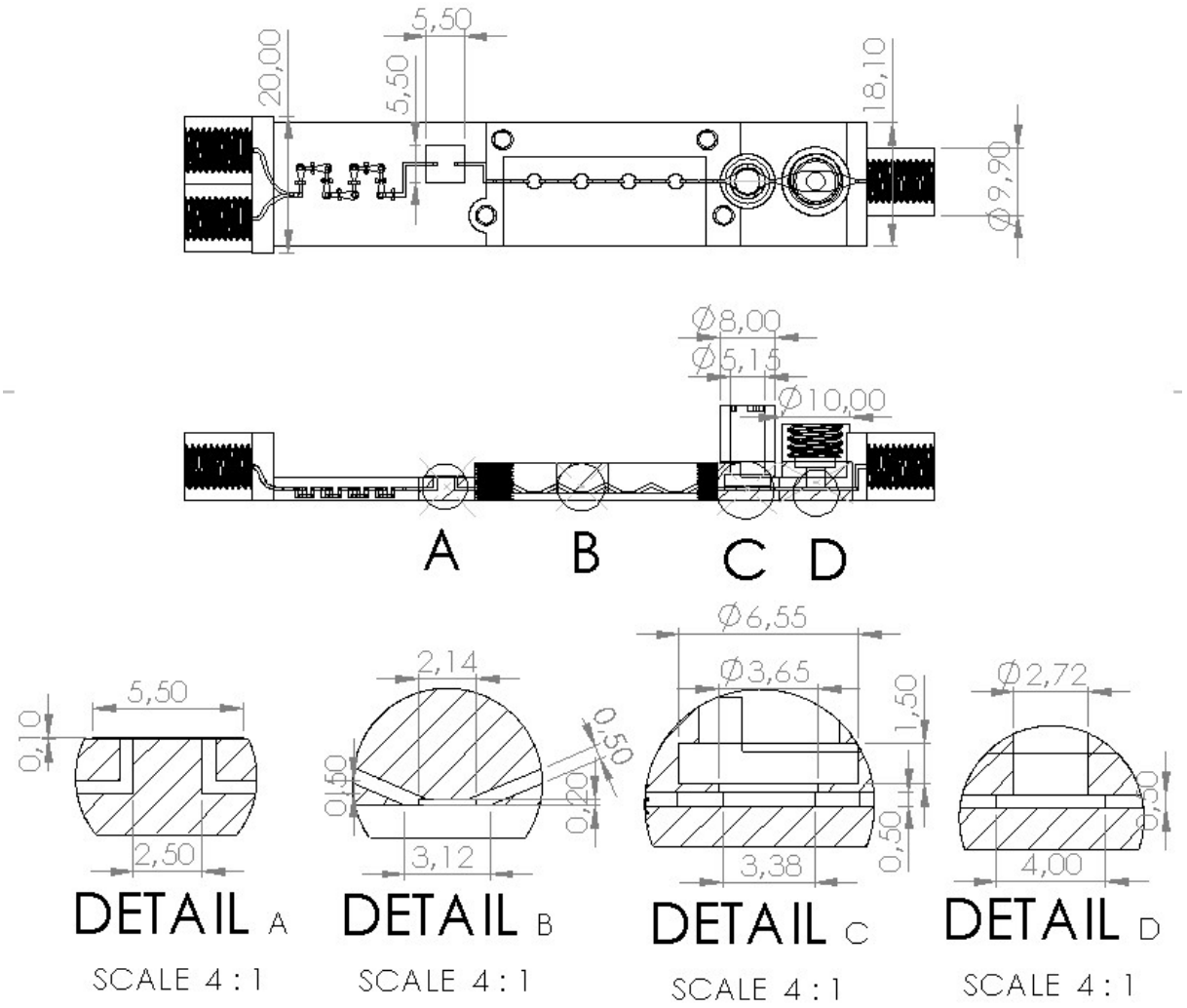

Fig. S4: Technical drawing of the microfluidic chip in top and side views. The detailed views show (from left to right) a magnification of the bubble-trap, the Au/PtB sensor chamber, the reference electrode chamber, and the oxygen SensorPlug chamber.

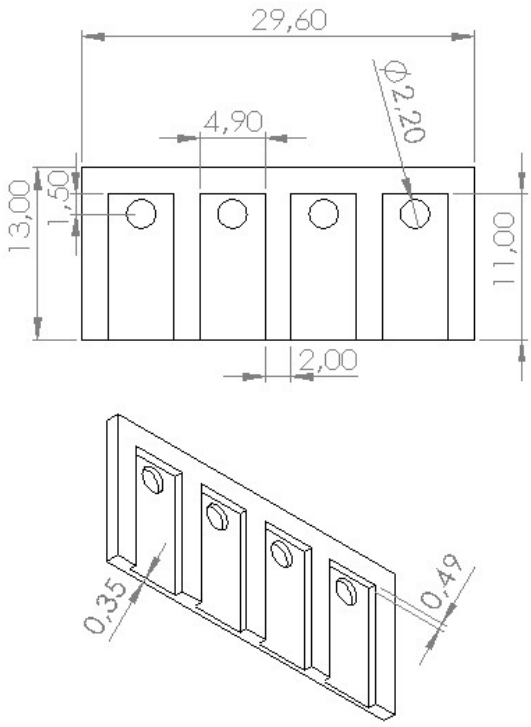

Fig. S5: Technical drawing of the 3D-printed gasket used to integrate four separated Au/PtB electrodes.

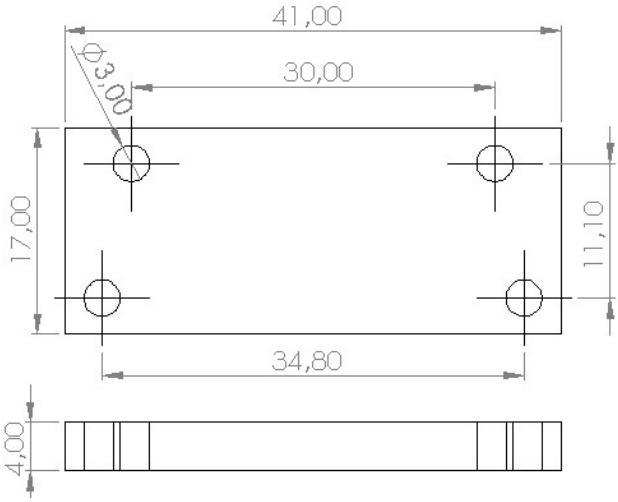

Fig. S6: Technical drawing of the 3D-printed lid used to apply pressure on the gasket.

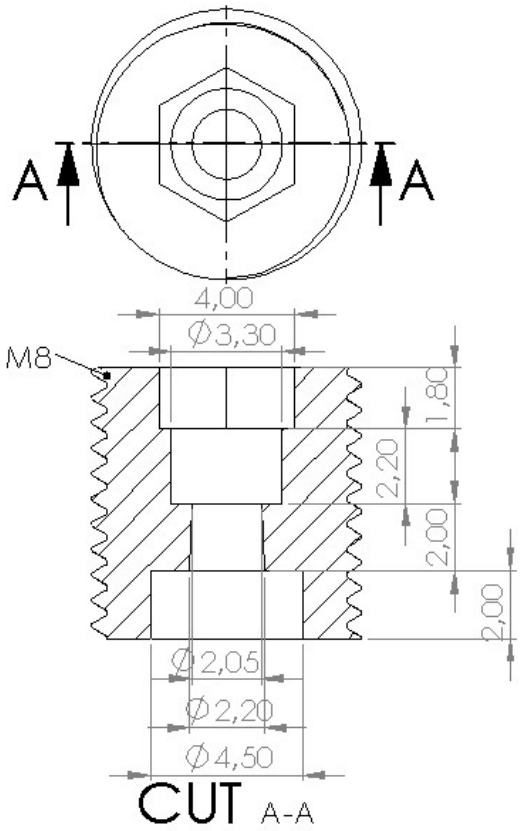

Fig. S7: Technical drawing of the 3D-printed screw cap for fixing SensorPlug inside its respective port.

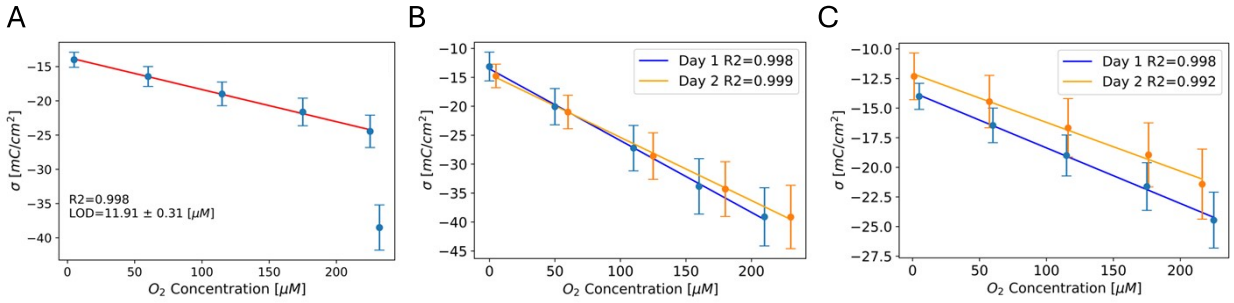

Fig. S8: (A) A full range charge density as a function of the optical oxygen sensor readings for PtB-coated electrodes. The graph shows a clear linear relationship at <230 µM and a significantly higher cathodic charge density in the PtB working electrode. Charge density as a function of the optical oxygen sensor using a 24h repeatability test for (B) Au and (C) PtB working electrodes. Day 1 is represented in blue, and day 2 is represented by orange markers and lines (-14.3- 0.11×dO_2 (day 1) and -14.5 - 0.12×dO_2 (day 2), and -13.7-0.05×dO_2 (day 1) and -12.1-0.04×dO_2 (day 2) for Au and PtB, respectively).